Transition between flocculation and percolation of a diffusion-limited cluster-cluster aggregation process using three-dimensional Monte Carlo simulation

Jean Christophe Gimel, Dominique Durand,* and Taco Nicolai
Laboratoire de Physico-Chimie Macromoléculaire, URA CNRS, Université du Maine, 72017 Le Mans Cedex, France
(Received 26 July 1994)

By Monte Carlo simulation we study the sol-gel transition of the diffusion-limited cluster aggregation process. We clearly show the absence of a critical concentration for gel formation and the existence of a well-defined gel time (t_g) with a power dependence on the volume fraction (ϕ_0): $t_g \propto \phi_0^{-2.85}$. We point out three main regimes of growth depending on the degree of overlap between the aggregates. In the very early stage when the aggregates have no overlap, the observed system behavior is in very good agreement with the predictions from the mean-field theory (flocculation regime). Close to the gel point there is a strong overlap between the aggregates and many critical quantities follow the same laws as those predicted by percolation theory. There is a smooth crossover between the two limiting situations due to a gradual interpenetration of the aggregates during the growth process. All throughout the growth process we found that networks built up by a dynamic random collision process have the same space filling properties as networks formed by a random distribution of matter.

INTRODUCTION

Most chemical systems form gels through an aggregation process of small particles or monomers, e.g., silica gels made from dilute solutions of tetramethoxysilicon in methanol,[1,2] globular proteins gels made by heat-induced aggregation,[3] and polymethacrylate gels made by radical copolymerization of methyl methacrylate (MMA) and ethylene glycol dimethacrylate (EGDMA).[4] Two main conceptual frameworks exist to describe the gelation process. The kinetic approach proposed by Smoluchowski[5,6] gives a description of the first stages of the aggregation process in the very dilute state, while the final stage close to the gel point has been viewed as a connectivity transition, which can be described in terms of the percolation model.[7,8] At present, no theory is available to describe the crossover between these two regimes. Computer simulation is probably the best alternative to study the complex intermediate regime. Using the Monte Carlo method it is possible to mimic the increasing connectivity from the beginning of the aggregation to the network formation.[9]

MODEL AND SIMULATION PROCEDURE

We have studied the gelation of the diffusion-limited cluster aggregation (DLCA) process on a finite-size cubic lattice with site length L. The DLCA model has been developed by Meakin[10] and Kolb, Botet, and Jullien.[11]

(a) The initial stage consists in randomly distributing N_0 monomers on the L^3 lattice sites, leading to a monomer concentration $\phi_0 = N_0/L^3$. Because it is a DLCA process, the following rule must be respected at any time during the simulation: if two monomers are near neighbors, they link up irreversibly and become part of the same cluster. The mass (m) of a cluster is defined as the number of monomers forming the cluster. So, isolated monomers are considered as clusters with $m = 1$.

(b) A Brownian motion is assumed for each cluster in the system, and the translational diffusion coefficient of a cluster is related to its mass as $D(m) \propto m^{-\alpha}$, where α is a positive mobility exponent. Big clusters consequently move slower than small ones. Supposing further that $D(m)$ is inversely proportional to the radius of the aggregate it follows that $\alpha = 1/d_f$, with d_f the fractal dimension of the aggregate. The present work has been realized with $\alpha = 0.55$, assuming that the clusters had a constant fractal dimension close to 1.8. In fact, as we will see below, the fractal dimension increases to 2.4–2.5 as the simulation progresses, so that the value of α is a bit overestimated. But it has been shown[12] that small variations of α, in this range, have nearly no influence on the kinetics. At each simulation step, one cluster is randomly selected and has a probability $m^{-\alpha}$ to move. If it moves, it is shifted one site in one of the six possible directions randomly chosen. The sticking rule must be checked and each collision must be solved. Whether it has moved or not, the simulation time t_{sim} is incremented by 1 and the physical time t by $1/N_c$, where N_c is the number of clusters present in the system at that time.

(c) The simulation ends when $N_c = 1$ or when a cluster joins two opposite sides of the system. In the latter case, we call that event the gel point, and t_g represents the physical gel time. Figure 1 shows the initial [Fig. 1(a)] and final [Fig. 1(b)] state of a simulation on a square lattice. This sequential algorithm is very convenient to mimic simultaneity of movements when $N_c \gg 1$. The physical time unit is the time needed for one monomer to move one lattice site and the length unit is the diameter of one monomer.

The initial stage (a) is, in fact, related to the classical percolation theory, and it is well known that on a site-cubic lattice, the critical concentration, ϕ_c, is about 0.31.[13] So, when L is large enough, any simulation started with $\phi_0 \geq \phi_c$ should give $t_g = 0$, since there is already a

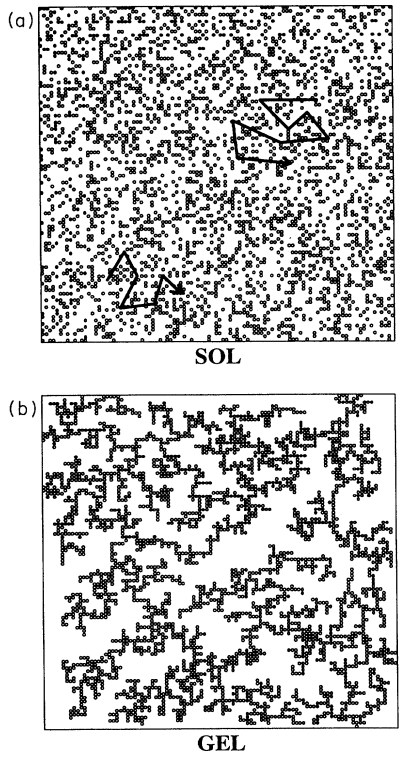

FIG. 1. Example of a simulation on a square lattice, $L=100$ ($\phi_0=30\%$). (a) Initial stage. (b) Gel point.

gel after having distributed $\phi_0 L^3$ monomers.

The computer simulations have been performed on an IBM 3090 located at CIRCE (Orsay, France). Typically, one simulation on a cubic lattice of 200^3 sites requires 100 megabytes of RAM and 12 h of CPU time.

RESULTS AND DISCUSSION

Sol-gel transition and critical behavior

If we suppose that ϕ_0 is slightly smaller than ϕ_c, there is no gel at $t=0$, but the clusters are strongly overlapping.[14] Moving just a few clusters can lead to the formation of the infinite network. When we decrease the initial concentration, the time needed to form a gel increases, but one may wonder if there is a critical concentration (ϕ_c^*) below which the dynamic DLCA process does not lead to a gel within a finite time span. ϕ_c^* will be called the dynamic critical concentration to be compared to the static ϕ_c in the percolation theory. Because we are working on finite-size lattices, we have to extrapolate our results to $L\to\infty$. To this end we have monitored the quantity $P(\phi_0,L)$, which represents the probability of forming a gel at concentration ϕ_0 on a cubic lattice with size L. $P(\phi_0,L)$ represents the number of trials leading to a gel divided by the total number of trials. This quantity has been evaluated as a function of ϕ_0 for different lattice sizes. The results, shown in Fig. 2, have been calculated on 100 trials, except for $L=5$ for which the number of trials is 10 000. In Fig. 2(a), we can see that the probability of forming a gel at a constant ϕ_0 increases with increasing lattice size. In addition, we can notice that the transition from $P(\phi_0,L)=0$ to 1 becomes more abrupt with increasing L. However, if $P(\phi_0,L)$ is plotted as a function of $\log_{10}(\phi_0)$, see Fig. 2(b), it is clear that the curves obtained for different values of L are similar and that decreasing L only leads to a shift to higher concentrations.

In order to quantify the size dependence, we can define $\Phi(p,L)$ as the concentration needed to form a gel with probability p on a lattice of size L. For any value of p, this quantity converges to ϕ_c^* as L increases.[15] Figure 3 shows on a log-log plot the evolution of $\Phi(p,L)$ as a function of L for p equal to 0.1, 0.5, and 0.9. $\Phi(p,L)$ has a power-law dependence on L with an exponent close to $-0{,}66$, irrespective of the value of p, which implies that the critical concentration ϕ_c^* is equal to zero.

Even though a gel is obtained at any concentration,

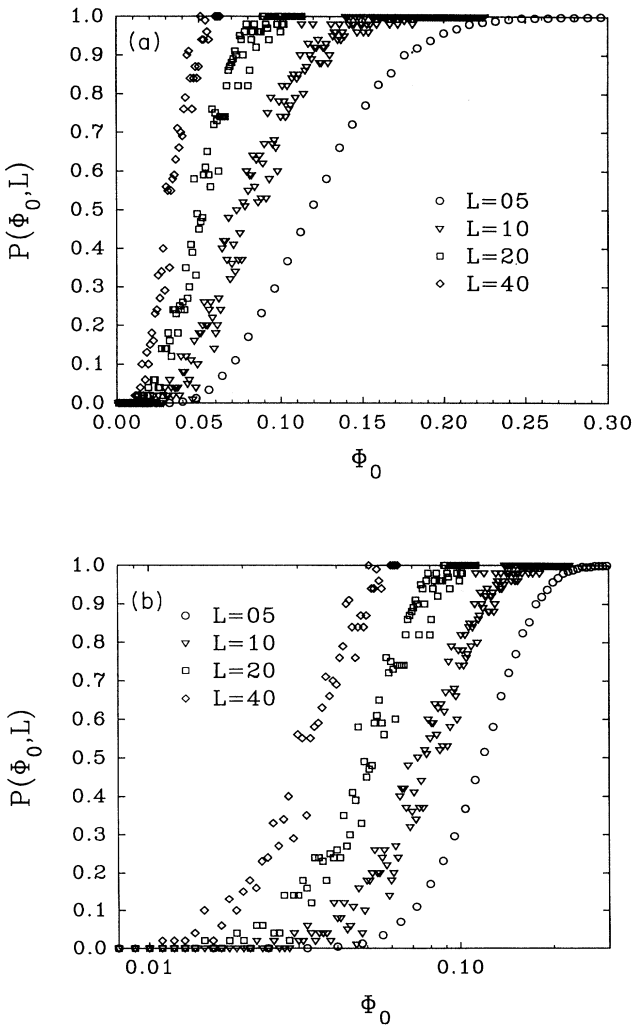

FIG. 2. (a) Lin-lin representation of the evolution of the gelation probability, $P(\phi_0,L)$ as a function of ϕ_0 for different lattice sizes L. (b) The same data in a lin-log representation.

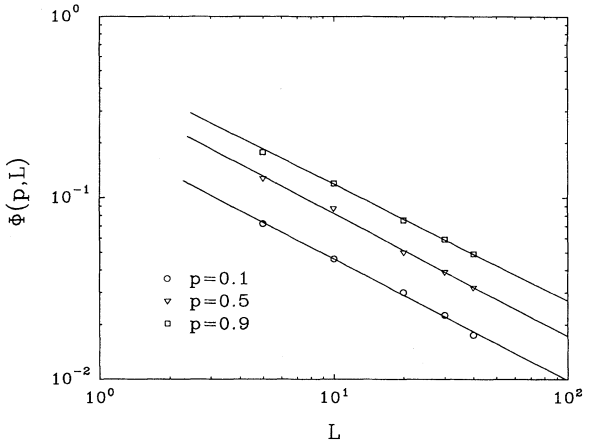

FIG. 3. Log-log representation of the evolution of $\Phi(p,L)$ as a function of L for different values of p. Solid lines represent linear least-squares fits and have a slope close to -0.66.

provided L is sufficiently large, the gel time becomes very long at low concentrations, and it is interesting to study t_g as a function of ϕ_0. Figure 4 shows the gel time distribution function for 100 trials at $\phi_0=0.1$ for various lattice sizes. The average gel time is not significantly different from one lattice size to another but the distribution narrows with increasing L. The sol-gel transition of the DLCA process occurs at a well-defined time if $L\to\infty$ or after averaging many simulations at finite L. Figure 5 shows the averaged gel time for $L=100$, as a function of the concentration, in the range $0.04<\phi_0<\phi_c$. Initial concentrations below 0.04 require large lattice sizes for $\Phi(p,L)$ to remain close to one which entails very long computing times and large memory. As expected, $t_g\to 0$ as $\phi_0\to\phi_c$. Moreover, t_g scales as $\phi_0^{-2.85}$ for $\phi_0<0.1$. Such a strong concentration dependence on the gel time is not predicted by any classical theory but has already been observed for different experimental systems.[16]

From the simulations, many physical quantities characterizing the kinetic aspect of the cluster growth and the size distribution of the clusters can be derived. Following Stauffer,[8] the mass distribution of the clusters $N(m)$ is

$$N(m)\propto m^{-\tau}f(m/m^*)\ , \tag{1}$$

where τ is the polydispersity exponent and $f(x)$ is a cutoff function at mass m^* decreasing faster than any power law. Assuming a stretched exponential cutoff function, Eq. (1) becomes

$$N(m)=Am^{-\tau}\exp[-(m/m^*)^{\beta}]\ . \tag{2}$$

By definition,

$$N_0=\int_1^{\infty} mN(m)dm$$
$$=A\frac{m^{*2-\tau}}{\beta}\int_{m^{*-\beta}}^{\infty} x^{(2-\tau)/\beta-1}\exp(-x)dx \tag{3}$$

with $x=(m/m^*)^{\beta}$. If $\tau<2$,

$$A=\frac{\beta N_0}{\Gamma[(2-\tau)/\beta]}m^{*\tau-2}\ . \tag{4a}$$

If $2<\tau<2+\beta$,

$$A=N_0(\tau-2)\ . \tag{4b}$$

We can note that Eq. (4a) is a function of m^*, while Eq. (4b) is independent of m^*.

The characteristic radius of an aggregate with mass m is

$$R(m)\propto m^{1/d_f}\ . \tag{5}$$

The weight average aggregation number (m_w) of the clusters is given by the normalized second moment of the cluster distribution:

$$m_w=\sum_{m=1}^{\infty} m^2N(m)\Big/\sum_{m=1}^{\infty} mN(m)\ . \tag{6}$$

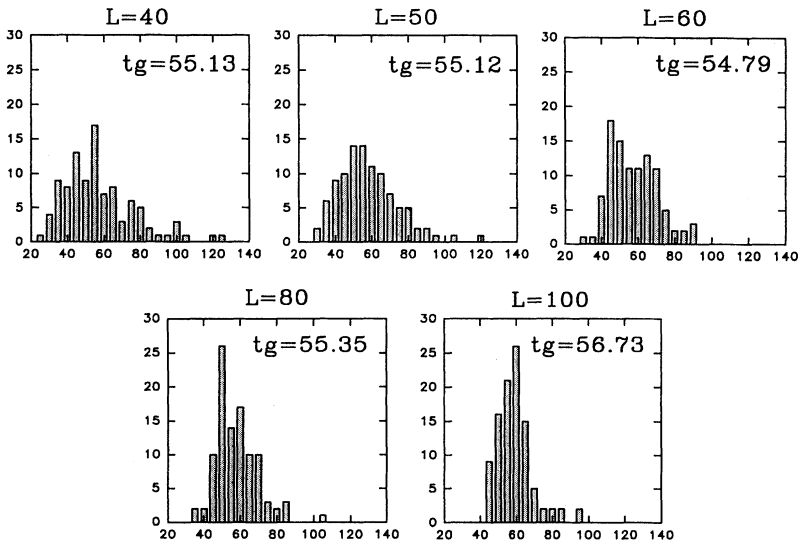

FIG. 4. Gel time distribution for different lattice sizes at $\phi_0=10\%$. The distribution has been evaluated using 100 trials.

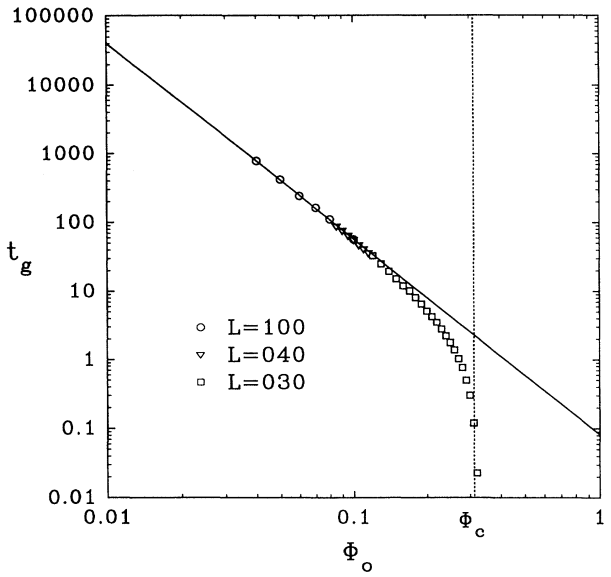

FIG. 5. Log-log representation of the evolution of the mean gel time as a function of ϕ_0, calculated using 100 trials with $L=100$. The solid line represents a linear fit for $\phi_0 \leq 10\%$ with slope -2.85 ± 0.03. The dotted line indicates the static critical concentration, $\phi_c=31.16\%$.

The number average aggregation number m_n and the polydispersity index (K) are given as

$$m_n = \sum_{m=1}^{\infty} mN(m) \Big/ \sum_{m=1}^{\infty} N(m) \tag{7}$$

and

$$K = \frac{m_w}{m_n} . \tag{8}$$

The sol-gel transition is mainly characterized by the divergence of the weight average aggregation number m_w of the clusters. The number average aggregation number m_n being finite at the gel point, the polydispersity index $K=m_w/m_n$ necessarily diverges. Figure 6 shows the evolution of K as a function of time for different concentrations. We have used $L=200$ for all the concentrations, except for $\phi_0=8\%$, where $L=190$. For the smallest concentrations 0.5 and 2%, the simulation cannot be run to the gel point because $P(\phi_0,L)<1$. We can notice that for $\phi_0=0.5\%$, after an initial aggregation period needed to build up a statistical distribution, the polydispersity index K becomes constant and equal to 2, as predicted by the mean-field theory.[17] In this so-called flocculation regime, the aggregates have a fractal dimension d_f close to 1.8 and $N(m)$ is given by Eq. (2) with $\tau=0$ and an exponential cutoff function.[18] For $\phi_0=2\%$, the polydispersity index stays a relatively short time in the flocculation regime ($K=2$) and then diverges. For the highest concentrations, K does not stabilize, but diverges directly. The mean-field theory can only predict the system behavior in the limit where collisions between

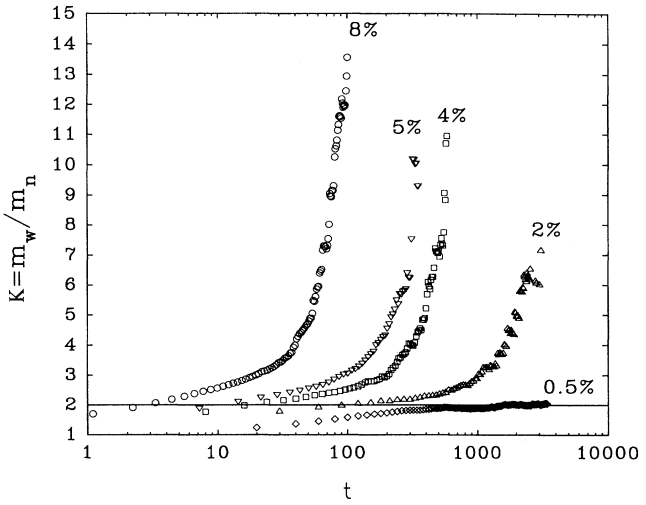

FIG. 6. Evolution of the polydispersity index as a function of time t at various concentrations with $L=200$ except at $\phi_0=8\%$, where $L=190$.

clusters are not correlated (statistically independent). This means that the average distance between clusters $r(t)$ must be very large compared to the average size of clusters $R(t)$. This condition is always achieved when $\phi_0 \to 0$, but when we deal with a finite nonzero concentration there is a characteristic time above which $R(t)$ equals $r(t)$ due to the fractal nature of the DLCA aggregates.[12] The mean-field approach is unable to describe the sol-gel transition, since it is not valid in a "congested" system. When $R(t)$ approaches $r(t)$, the space filling appears to be an important parameter, which can be used to characterize the whole aggregation process.

Space filling

Let V_i be the volume fraction occupied by the ith cluster. V_i can be defined as the volume of the smallest rectangular box containing the cluster divided by L^3. In order to monitor the space filling all along the simulation, we can calculate two different volume fractions, the effective (V_{eff}) and the cumulative (V_{cum}), defined by

$$V_{\text{eff}} = \bigcup_{i=1}^{N_C} V_i , \tag{9}$$

$$V_{\text{cum}} = \sum_{i=1}^{N_C} V_i = \frac{B}{L^3} \sum_{m=1}^{\infty} R_g(m)^3 N(m) , \tag{10}$$

where R_g is the radius of gyration of an aggregate, and B is a proportionality constant. From the simulation we find $B=14$. Using Eq. (10) it is possible to calculate V_{cum} for real systems and thus to apply the simulation results reported here. Replacing the sum in Eq. (10) by an integral, we obtain

$$V_{\text{cum}} \propto A m^{*3/d_f-\tau+1} \int_{m^{*-\beta}}^{\infty} x^{(3/d_f-\tau+1)/\beta-1} \times \exp(-x)dx . \tag{11}$$

In the flocculation regime of the DLCA process, using

$\tau=0$, $A \propto No/m^{*2}$ and $m^* \propto m_w$ we have

$$V_{\text{cum}} \propto \phi_0 m_w^{3/d_f-1} . \tag{12}$$

In the vicinity of the gel point for a percolation process, using the hyperscaling law $3/d_f-\tau+1=0$,[8] we get

$$V_{\text{cum}} \propto \ln(m^*)-\frac{\gamma}{\beta} , \tag{13}$$

where γ is the Euler constant ($\gamma=0.577$). A schematic representation of V_{eff} and V_{cum} for the two-dimensional case is shown in Fig. 7.

We can also calculate the distribution function of space occupation, $\Omega(n)$, defined as the volume fraction under the influence of exactly n clusters. With this formalism, we have

$$V_{\text{eff}}=\sum_{n=1}^{\infty} \Omega(n) \tag{14}$$

and

$$V_{\text{cum}}=\sum_{n=1}^{\infty} n\cdot\Omega(n) \tag{15}$$

with

$$\sum_{n=0}^{\infty} \Omega(n)=1 .$$

The void volume fraction of the system is simply equal to $1-V_{\text{eff}}$ or $\Omega(0)$. V_{eff} represents the volume fraction under the influence of at least one cluster. When there is no overlap between clusters, $V_{\text{eff}}=V_{\text{cum}}$, which is the case during the first stage of the process; otherwise $V_{\text{eff}}<V_{\text{cum}}$. At the gel point, $V_{\text{eff}}=1$, as we can see in Fig. 8, where the evolution of V_{eff} is plotted as a function of time for different ϕ_0.

The polydispersity index (K) is plotted as a function of $(1-V_{\text{eff}})/V_{\text{eff}}$ in Fig. 9 on a lin-log scale. This representation shows well the limiting behavior of both $V_{\text{eff}}\to 1$ and $V_{\text{eff}}\to 0$. Apart from the initial aggregation stage, all data fall on the same master curve, showing the universal behavior of the aggregation process independent of ϕ_0

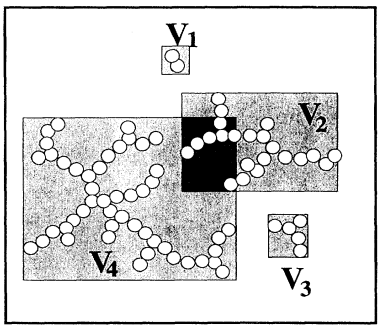

$$V_{\text{cum}} = V_1 + V_2 + V_3 + V_4$$
$$V_{\text{eff}} = V_1 + V_2 + V_3 + V_4 - V_2 \cap V_4$$

FIG. 7. Schematic representation in $2d$ of V_{eff} and V_{cum}.

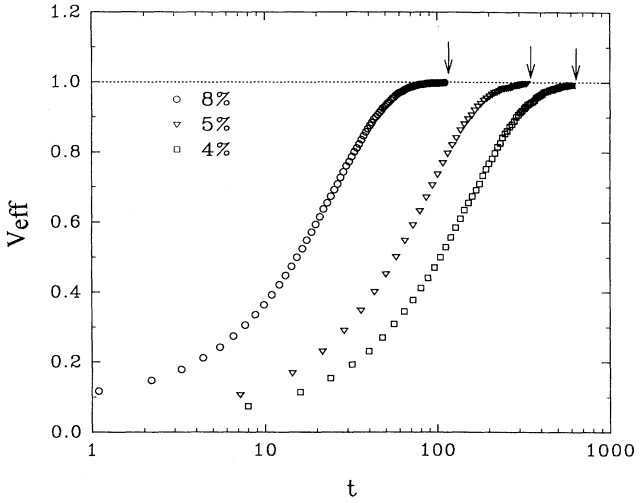

FIG. 8. Evolution of V_{eff} as a function of time for different ϕ_0. Arrows indicate the gel point.

and revealing the pertinence of the parameter V_{eff} to monitor the advancement of the reaction. We can also notice in Fig. 9 that the flocculation regime is only valid for $V_{\text{eff}}<0.1$.

The universal behavior of the aggregation process does not only appear through the evolution of the polydispersity index, but also through the way the space is filled; see Fig. 10. In Fig. 10(a), we see that all the couples (V_{eff}, V_{cum}) fall on the same master curve, independent of ϕ_0. The initial points (V_{eff}, V_{cum}) at $t=0$ fall on the same curve and result from a static percolation process. Additional static percolation data were obtained in the range $0.01<\phi_0<\phi_c$ by averaging results of 100 trials using a lattice of size $L=150$, and are represented by the filled symbols. From Fig. 10(b), it is clear that all along the aggregation, the space filling is the same whether it is a

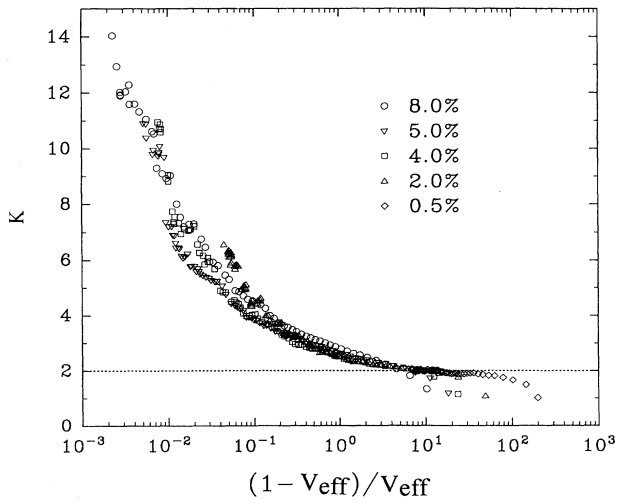

FIG. 9. Same data as Fig. 6 plotted as a function of $(1-V_{\text{eff}})/V_{\text{eff}}$.

result of a dynamic DLCA process or a static percolation process. We can also notice that V_{cum} diverges as the logarithm of $(1-V_{eff})^{-1}$ for $V_{cum}>2$. The degree of overlap is shown in Fig. 11, where $\Omega(n)$ is plotted at different stages of the DLCA process. It is clear that even very close to the gel point, the average degree of interpenetration related to the occupied space (V_{cum}/V_{eff}) remains rather low, and the degree of overlap is not uniform over the whole space. Figure 11(b) shows that the space occupation is the same in the case of static percolation. A more detailed investigation of heterogeneity of the space filling is important for an understanding of structure of the final gel and is currently being conducted.

If we monitor the evolution of m_w as a function of $(1-V_{eff})$, we notice once more the similarity with percolation theory; see Fig. 12. Figure 12(a) shows that m_w diverges as a power law of $(1-V_{eff})$. In the DLCA process the same space filling can be obtained with different initial concentrations, but for the same space filling m_w increases with decreasing ϕ_0. The limiting slope is close to -0.75 for the dynamic DLCA and appears slightly smaller for the static percolation. However, if we take into account the finite-size scaling effects, still important on a lattice of size $L=150$ (see below), the limiting slope is the same. In order to distinguish the behavior at small values of V_{eff}, the data have been represented in Fig. 12(b) as a function of $(1-V_{eff})/V_{eff}$, showing again that the initial points of the dynamic simulations are the results of a static percolation process. In percolation theory the parameter governing the approach to the gel point is $\epsilon=(\phi_c-\phi_0)/\phi_c$. For a quantitative comparison with percolation theory we need to correlate $(1-V_{eff})$ with ϵ. Figure 13(a) shows the evolution of $(1-V_{eff})$ as a function of ϵ for percolation on different lattice sizes demonstrating the influence of finite-size scaling effects. The

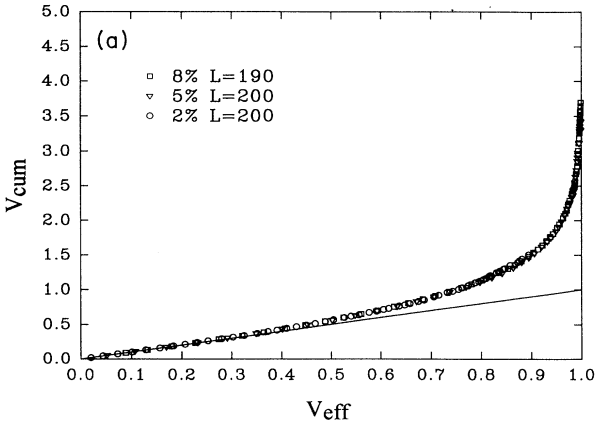

FIG. 10. (a) Evolution of V_{cum} as a function of V_{eff} for different ϕ_0. The solid line corresponds to $V_{cum}=V_{eff}$. (b) Comparison of the evolution of V_{cum} as a function of $(1-V_{eff})/V_{eff}$ for DLCA and static site percolation. The straight line represents a linear least-squares fit to the site percolation data (filled symbols) for $(1-V_{eff})<0.03$.

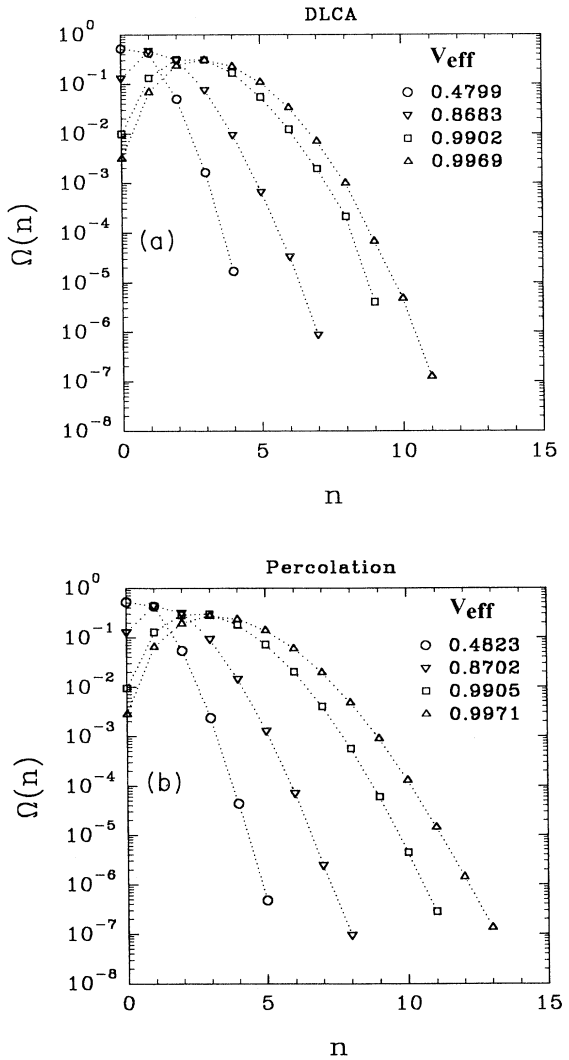

FIG. 11. (a) A semilogarithmic representation of the evolution of $\Omega(n)$ as a function of m at various aggregation extents for the DLCA process with $L=200$ and $\phi_0=7.4\%$. (b) A semilogarithmic representation of the evolution of $\Omega(n)$ as a function of m at various values of ϕ_0 for the static site percolation process with $L=150$.

corrective term $aL^{-1/\nu}$ used in Fig. 13(b) takes these effects into account.[13,22] ν (close to 0.88) is the exponent describing the divergence of the maximum cluster size in the neighborhood of the gel point and a is a constant. We have finally $(1-V_{\text{eff}}) \propto \epsilon^{2.36}$, which gives $m_w \propto \epsilon^{-1.77}$, in very good agreement with the value -1.80 predicted by the percolation theory. In addition, in the percolation theory, we have $m_w \propto \epsilon^{-\gamma}$ ($\gamma=1.80$) and $m^* \propto \epsilon^{-1/\sigma}$ ($\sigma=0.45$), which leads to

$$m_w \propto m^{*0.81} . \tag{16}$$

Equation (16) and the experimental relation $(1-V_{\text{eff}}) \propto m_w^{-1/0.75}$ for $m_w \gg 1$ (Fig. 12) leads to

$$(1-V_{\text{eff}}) \propto m^{*-1.1} . \tag{17}$$

Using this result in Eq. (13), we find $V_{\text{cum}} \propto -\ln(1-V_{\text{eff}})$ for large m^*, which is confirmed by the simulation results shown in Fig. 10(b).

If we assume that the m_w required to fill up a certain space scales with the initial concentration, we can try to renormalize the data by the parameter ϕ_0^{δ}. Figure 14 shows that the best master curve is obtained for δ close to 1.3, and if we correct the percolation data for finite-scaling effects, a near perfect superimposition is obtained for all the data, except at the very beginning of each DLCA simulation. The relationship $m_w \phi_0^{\delta} = Cte$ means that in such a stochastic process, there exists an infinite number of couples (m_w, ϕ_0) which give the same space filling. In fact, for $V_{\text{eff}} < 0.1$, we are in the flocculation regime, and Eq. (12) implies $\delta = d_f/(3-d_f)$. The experi-

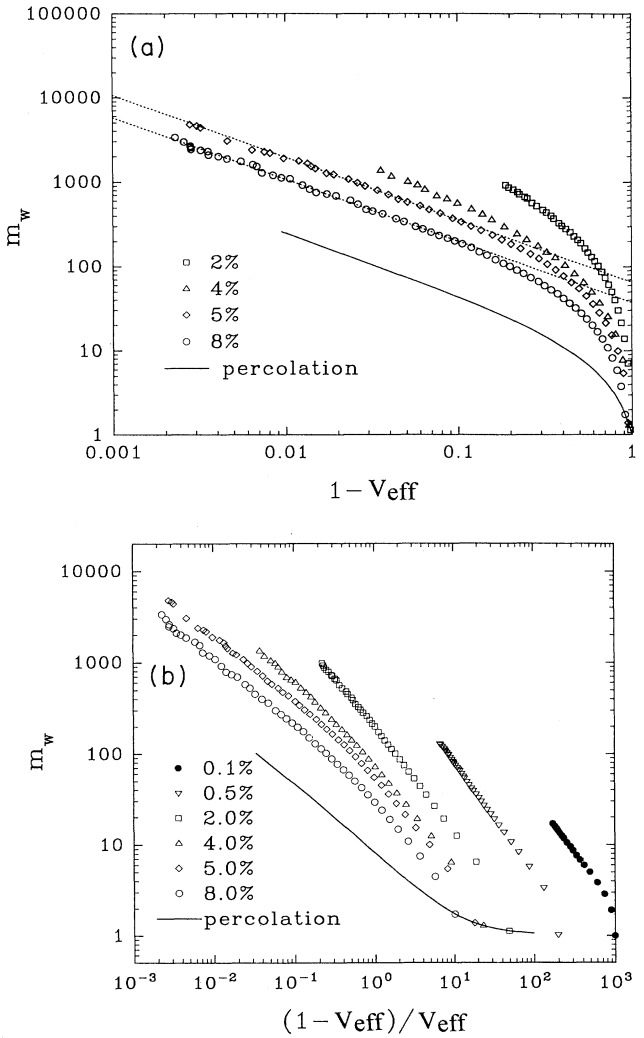

FIG. 12. (a) Log-log representation of the evolution of m_W as a function of $(1-V_{\text{eff}})$ for DLCA at various values of ϕ_0 with $L=200$ (except at $\phi_0=8\%$, where $L=190$) and static site percolation with $L=150$. Dotted lines represent linear least-squares fits for ϕ_0 equal to 5 and 8% and $V_{\text{eff}} > 90\%$. Their slope is close to -0.75. (b) Log-log representation of the evolution of m_W as a function of $(1-V_{\text{eff}})/V_{\text{eff}}$ for DLCA and static site percolation.

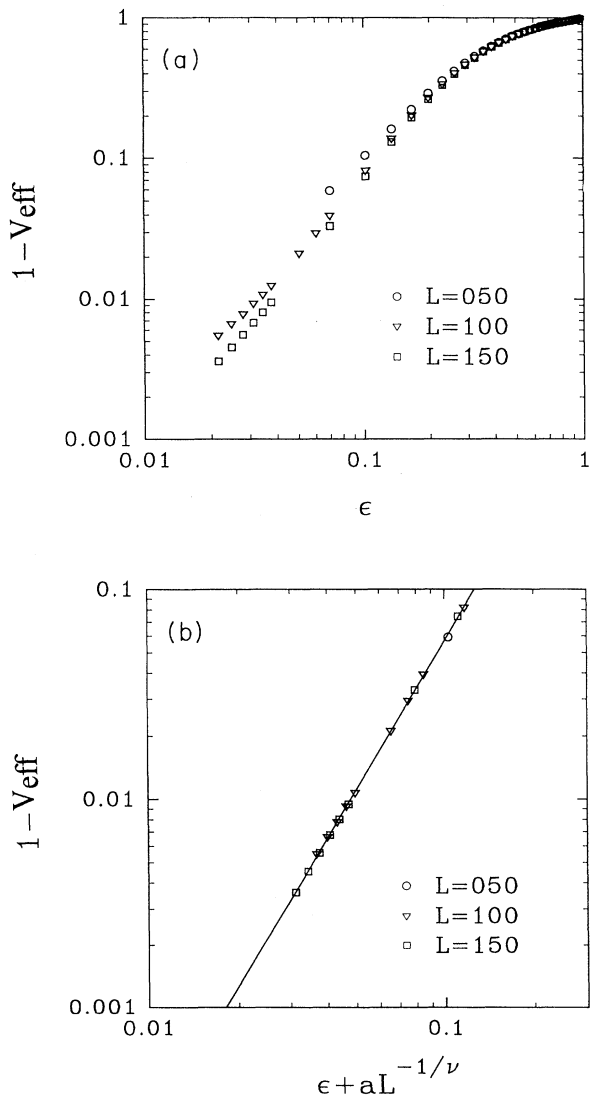

FIG. 13: (a) Double logarithmic representation of $(1-V_{\text{eff}})$ vs ϵ for site percolation on various lattice sizes. We have used $\phi_c=0.3116$ to calculate ϵ. (b) Same data after correction for finite-size scaling effects (see text), the straight line represents a linear least-squares fit for $(1-V_{\text{eff}}) < 10\%$ with slope 2.36 ± 0.01.

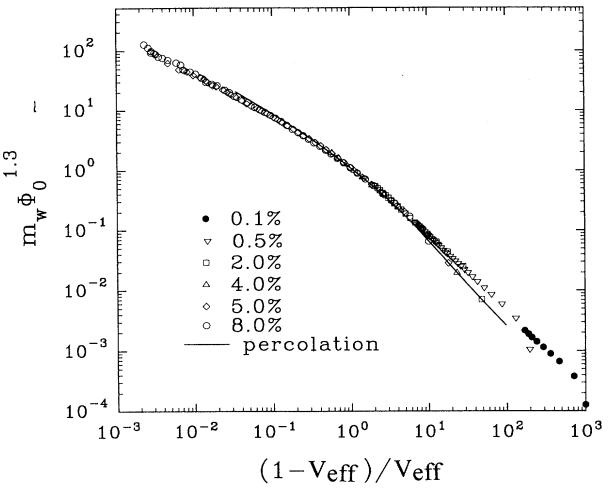

FIG. 14. Double logarithmic representation of $m_W\phi_0^{1.3}$ as a function of $(1-V_{\text{eff}})/V_{\text{eff}}$ at various values of ϕ_0.

mental value of $\delta \cong 1.3$ leads to a d_f value closed to 1.70 which is in good agreement with the experimental values reported in the literature for the DLCA process.[12,18] However, it is noticeable that this scaling relation is still valid outside the flocculation regime ($V_{\text{eff}} > 0.1$), where both d_f and τ vary with V_{eff} (see below).

Cluster distribution and fractal structure of the clusters

The crossover observed for this aggregation process from the flocculation regime to the so-called percolation regime implies that strong modifications of both the cluster distribution and fractal dimension occur during the aggregation process. In the flocculation regime, the fractal dimension is close to 1.7 and according to percolation theory $d_f = 2.5$ at the gel point. The exponent τ characterizing the mass distribution is equal to zero in the flocculation regime and 2.2 at the gel point according to percolation theory.

Pair correlation function. We have determined the pair-correlation function $[g(r)]$ as a function of the distance r between monomers of the largest aggregate of the system grown close to the gel point on a lattice with size 200 and with monomer concentration 7.4%. The aggregate contained 177 293 monomers and 1×10^9 out of 1.57×10^{10} possible pairs were randomly selected to calculate $g(r)$. $g(r)$ is normalized to give $4\pi\int r^2 g(r)dr = m$ so that

$$R_g^2 = \frac{1}{2m}\int 4\pi r^4 g(r)dr \ . \tag{18}$$

Using $m = 177\,293$, we find $R_g = 89.17$, which agrees with the value 89.18 obtained by direct calculation using $R_g^2 = (1/m)\sum_{i=1}^{m} r_i^2$ with r_i the distance between monomer i and the center of mass of the aggregate. For fractal objects at distances where short-range excluded volume effects are no longer felt, $g(r)$ can be written as

$$g(r) \propto r^{d_f - 3}\exp[-(r/\xi)^{\gamma}] \ . \tag{19}$$

We have chosen a stretched exponential to describe the cutoff at $r > \xi$. A nonlinear least-squares fit to Eq. (19) fixing $d_f = 2.5$ gave $\xi = 122 \pm 1$ and $\gamma = 2.18 \pm 0.05$. The result is shown in Fig. 15, and it is clear that for $r > 20$ we obtain an excellent agreement with Eq. (19). At smaller r deviations are expected due to excluded volume effects.[19] The value of γ is maybe slightly overestimated due to the finite lattice size (419 monomers are situated at the edge of the lattice), but it is larger than unity, which implies that $g(r)$ has a sharper cutoff than a simple exponential. A value close to 2 is also found for aggregates obtained in DLCA and reaction-limited cluster aggregation simulation.[20,21] Using Eqs. (18) and (19), the following relation can be derived:

$$R_g^2 = \xi^2 \frac{\Gamma[(d_f+2)/\gamma]}{2\Gamma(d_f/\gamma)} \ . \tag{20}$$

Using $d_f = 2.5$, $\gamma = 2.18$, and $\xi = 122$, we find $R_g = 90.5$. These results show that the short-range excluded volume effects have little influence on the value of ξ and R_g. As the aggregate we have studied was the largest in the ensemble with $m > m^*$, one might expect it to have the structure of a lattice animal with $d_f = 2$.[8,22] However, there is no reason why an aggregate should stay among the very small population of lattice animals during the whole period of its growth. In fact, the time spent in the regime where $m > m^*$ is relatively short and the influence on its structure is negligible.

Size distribution. We have studied the aggregation number distribution at four different stages of the simulation on a lattice with $L = 200$ and monomer concentration 7.4%. Some characteristics of the four distributions are given in Table I. The aggregation number distribu-

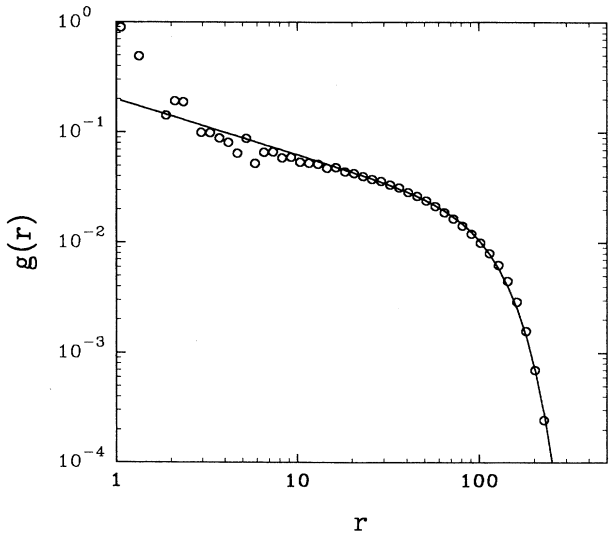

FIG. 15. Double logarithmic representation of the pair-correlation function $g(r)$ as a function of r for the largest cluster of the system close to the gel point ($L = 200$, $\phi_0 = 7.4\%$). The experimental data have been smoothed using 50 classes between $r = 1$ and 287 of equal size on the logarithmic scale. The solid line corresponds to a fit using Eq. (18).

TABLE I. Characteristics of the aggregate distribution at four stages of the simulation.

	V_{eff}	V_{cum}	m_n	m_w	m_z	m^+
1	0.2998	0.3016	6.2	13	24	
2	0.7945	1.117	32	110	250	250
3	0.9523	1.879	74	370	890	500
4	0.9945	3.862	330	7600	22 000	1200

tions are plotted in Fig. 16. From Eq. (1) it follows that in a log-log representation the slope for $m \ll m^*$ is equal to $-\tau$. In all cases we find that the initial slope is close to zero, in agreement with DLCA. Closer to the gel point the slope approaches 2.2 for large m, as expected from percolation theory. The aggregation number distributions of these two limiting cases are shown in Fig. 17. In the early stage of the aggregation the aggregates do not interpenetrate and the distribution is close to that expected for DLCA. After this stage the largest aggregates will grow by a percolation process, while the smallest aggregates continue to grow by a DLCA process. The transition between the two regimes is expected to occur at m^+ where

$$\sum_{i=1}^{m^+} V(m)N(m) \approx 1 \tag{21}$$

with $V(m)$ the volume fraction of a cluster with aggregation number m. For $m \ll m^+$ the distribution will be that of DLCA and for $m \gg m^+$ it will be that of percolating clusters. Values of m^+ are given in Table I, except for the distribution at the earliest stage, where $V_{\text{cum}} < 1$. With increasing aggregation the number of monomers decreases so that larger clusters are needed to fill up the space, which explains why m^+ increases. It is clear that the transition zone is large, and it is difficult to fulfill the conditions $m^+ \ll m \ll m^*$ in Monte Carlo simulations. The cutoff at large m is well described by $\exp(-m/m^*)^\beta$ with β close to unity and m^* close to the z-average aggregation number (m_z) given in Table I. We cannot distinguish between an exponential cutoff, as is expected for DLCA and the cutoff function found for percolating clusters.[23,24]

In Fig. 18 the aggregation number is plotted as a function of the radius of gyration. Within the scatter of the data the relation between m and R_g is the same for the

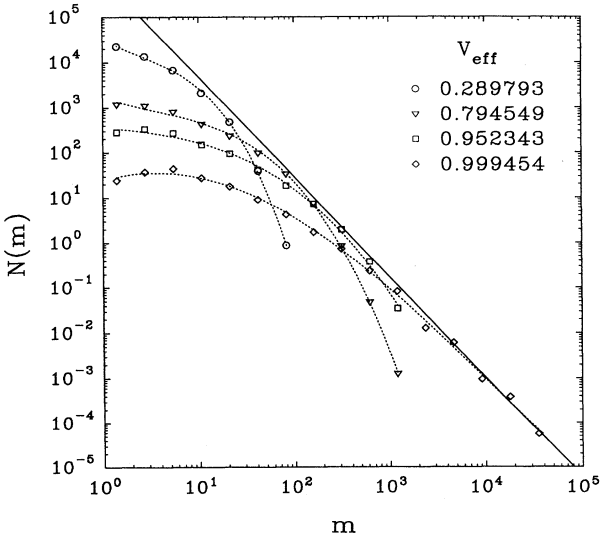

FIG. 16. Evolution of cluster size distribution for various aggregation extents for a DLCA simulation ($L=200$, $\phi_0=7.4\%$). The experimental data have been smoothed using 16 classes between $m=1$ and 5×10^4 of equal size on the logarithmic scale. The smoothing used is mass conservative [$\sum mN(m)=No$]. The straight line indicates the limiting slope, -2.2, expected from percolation theory.

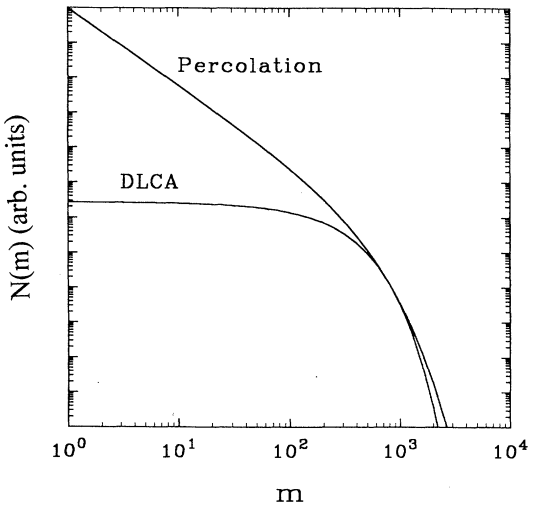

FIG. 17. Theoretical cluster distribution in the flocculation regime of a DLCA process and for percolation close the gel point. Both distributions have the same cutoff mass $m^*=1000$.

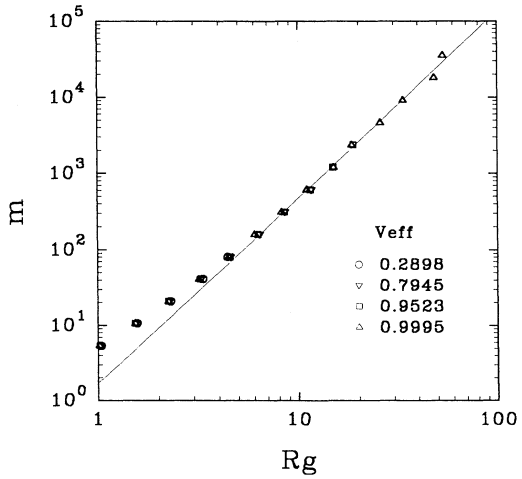

FIG. 18. Double logarithmic representation of the mass m of the clusters as a function of their radius of gyration at the gel point with $\phi_0=7.4\%$ and $L=200$. The experimental data have been smoothed using 16 classes between $m=1$ and $m=5\times10^4$ of equal size on the logarithmic scale. The solid line with slope 2.5 represents the dependence expected from percolation theory.

different stages of the growth. In a log-log representation the slope corresponds to d_f. Again we observe a transition from a dependence expected for DLCA to that expected for percolation.

One might expect a single aggregate to show a similar double structure, i.e., a smaller fractal dimension at short length scales corresponding to DLCA aggregates and a larger d_f at longer distances. However, the transition between the two structures depends on the history of the aggregate. If the aggregate reaches the percolation regime early in the aggregation process, the transition will be situated at small r. If it reaches the percolation regime, later the transition will occur at larger distances. The structure factor in the preceding section was calculated for the largest aggregate in the ensemble so that the transition is expected to have occurred at an early stage. This explains why the aggregate has a structure very close to that of percolating cluster even at short distances.

CONCLUSION

The main features pointed out by this study are the following. (1) There exists no critical concentration for gel formation. (2) The sol-gel transition is quite well defined in this dynamic DLCA process and occurs at a well-defined time depending only on the concentration. (3) The space filling monitored by the effective volume fraction V_{eff}, occupied by clusters, appears as the relevant parameter governing the system behavior. (4) Three regimes can be pointed out. (i) When $V_{\text{eff}} < 0.1$, the kinetic aggregation is described by mean-field theory giving a polydispersity index of the clusters $K = 2$ and a fractal dimension close to 1.8. (ii) For $V_{\text{eff}} > 0.9$, many critical quantities (weight average aggregation number, cumulative volume fraction, polydispersity index, etc.) follow the same scaling laws as those predicted by percolation theory in the vicinity of the gelation threshold. In addition, above a certain length scale, the fractal dimension of the clusters is close to the predicted value of the percolation theory. Also, the exponent governing the cluster distribution tends to 2.2 as predicted by percolation theory for the larger clusters in the vicinity of the gel point. (iii) The intermediate regime $0.1 < V_{\text{eff}} < 0.9$ is very large and corresponds to a system of partially interpenetrating clusters.

(5) Finally, whatever the initial concentration, above a certain length scale depending on ϕ_0 and m_w, the space filling mechanism involved in this dynamic growth is the same as the one generated by a static site percolation. Below this characterization length scale, the aggregates grow in the flocculation regime. Networks build up by a dynamic random collision process have the same space filling properties as networks formed by a random distribution of matter. The underlying reason for this universal manner to fill the space might be the intrinsic stochastic nature of both processes.

*Author to whom correspondence should be addressed.

[1]J. E. Martin and K. D. Keefer, Phys. Rev. Lett. **34**, 4988 (1986).
[2]J. E. Martin and J. P. Wilcoxon, Phys. Rev. A **34**, 1803 (1987).
[3]J. C. Gimel, D. Durand, and T. Nicolai, Macromol. **27**, 583 (1994).
[4]L. Fang, W. Brown, and C. Konak, Macromol. **24**, 6839 (1991).
[5]M. Von Smoluchowski, Z. Phys. **17**, 585 (1916).
[6]M. Von Smoluchowski, Z. Phys. Chem. **92**, 129 (1917).
[7]P. G. de Gennes, *Scaling Concepts in Polymer Chemistry* (Cornell University Press, London, 1979).
[8]D. Stauffer, *Introduction to Percolation Theory* (Taylor and Francis, London, 1985).
[9]D. Durand, in *Polymer Yearbook,* edited by R. A. Pethrick (Harwood Academic, City, 1986), Vol. 3, pp. 229–253.
[10]P. Meakin, Phys. Rev. Lett. **51**, 1119 (1983).
[11]M. Kolb, R. Botet, and R. Jullien, Phys. Rev. Lett. **51**, 1123 (1983).
[12]T. Vicsek, *Fractal Growth Phenomena* (World Scientific, London, 1989).
[13]D. Stauffer and A. Aharony, *Introduction to Percolation Theory,* 2nd ed. (Taylor and Francis, London, 1992).
[14]M. Daoud, Prog. Reaction Kinetics **15**, 1 (1989).
[15]J. P. Clerc, G. Giraud, J. Roussenq, R. Blanc, J. P. Carton, E. Guyon, H. Ottavi, and D. Stauffer, Ann. Phys. (Paris) **8**, 5 (1983).
[16]S. B. Ross Murphy, Int. J. Biol. Macromol. **3**, 315 (1981).
[17]R. J. Cohen and G. B. Benedeck, J. Chem. Phys. **86**, 3696 (1982).
[18]R. Jullien and R. Botet, *Aggregation and Fractal Aggregates* (World Scientific, Singapore, 1987).
[19]A. Hasmy, M. Foret, J. Pelous, and R. Jullien, Phys. Rev. B **48**, 9345 (1993).
[20]R. Klein, D. A. Weitz, M. Y. Lin, H. M. Lindsay, R. C. Ball, and P. Meakin, Prog. Colloid Polymer Sci. **81**, 161 (1990).
[21]T. Nicolai, D. Durand, and J. C. Gimel, Phys. Rev. B **50**, 16 357 (1994).
[22]J.-F. Gouyet, *Physique et Structures Fractales* (Masson, Paris, 1992).
[23]D. Stauffer, in *On Growth and Form,* edited by H. E. Stanley and N. Ostrowsky (Martinus Nijhoff, Dordrecht, 1986), pp. 79–100.
[24]P. L. Leath, Phys. Rev. B **14**, 5046 (1976).

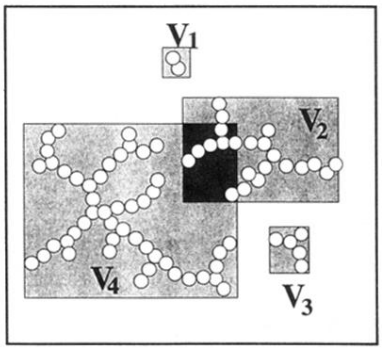

$$V_{cum} = V_1 + V_2 + V_3 + V_4$$

$$V_{eff} = V_1 + V_2 + V_3 + V_4 - V_2 \bigcap V_4$$

FIG. 7. Schematic representation in $2d$ of V_{eff} and V_{cum}.